

Article

Graphene-Infused Hybrid Biobattery–Supercapacitor Powered by Wastewater for Sustainable Energy Innovation

Sambhu Sapkota ¹, Matthew Hummel ² , Mahzuzah Zahan ¹, Sushma P. Karanam ¹, Jejal Bathi ³ ,
Namita Shrestha ⁴, Zhengrong Gu ² and Venkataramana Gadhamshetty ^{1,5,*}

¹ Department of Civil and Environmental Engineering, South Dakota Mines, 501 E Saint Joseph Blvd., Rapid City, SD 57701, USA; ssapkota2134@protonmail.com (S.S.); mahzuzah.zahan@mines.sdsmt.edu (M.Z.); sushmapriyanka.k@gmail.com (S.P.K.)

² Department of Agricultural and Biosystems Engineering, South Dakota State University, 2100 University Station, Brookings, SD 57701, USA

³ Department of Civil and Chemical Engineering, University of Tennessee at Chattanooga, 1615 McCallie Ave., Chattanooga, TN 37403, USA

⁴ Department of Civil and Environmental Engineering, Rose-Hulman Institute of Technology, 5500 Wabash Ave., Terre Haute, IN 47803, USA; namitasth411@gmail.com

⁵ 2-Dimensional Materials for Biofilm Engineering Science and Technology (2D-BEST) Center, South Dakota Mines, SD 57701, USA

* Correspondence: venkataramana.gadhamshetty@sdsmt.edu; Tel.: +1-605-394-1997

Abstract: Human society annually produces nearly 100 billion gallons of wastewater, containing approximately 3600 GWh of energy. This study introduces a proof of concept utilizing graphene materials to extract and instantly store this energy. A hybrid device, mimicking a microbial fuel cell, acts as both a battery and supercapacitor. Wastewater serves as the electrolyte, with indigenous microorganisms on the graphene electrode acting as biocatalysts. The device features a capacitive electrode using a 3D nickel foam modified with a plasma-exfoliated graphene mixture. Compared to controls, the Gr/Ni configuration shows a 150-fold increase in power output (2.58 W/m²) and a 48-fold increase in current density (12 A/m²). The Gr/Ni/biofilm interface demonstrates outstanding charge storage capability (19,400 F/m²) as confirmed by electrochemical impedance spectroscopy. Microscopy, spectroscopy, and electrochemical tests were employed to elucidate the superior performance of Gr/Ni electrodes. Ultimately, the capacitive energy extracted from wastewater can power small electrical equipment in water infrastructure, addressing energy needs in remote regions without access to a typical power grid.

Keywords: biobattery; battery–supercapacitor; microbial fuel cells; graphene



Citation: Sapkota, S.; Hummel, M.; Zahan, M.; Karanam, S.P.; Bathi, J.; Shrestha, N.; Gu, Z.; Gadhamshetty, V. Graphene-Infused Hybrid Biobattery–Supercapacitor Powered by Wastewater for Sustainable Energy Innovation. *Inorganics* **2024**, *12*, 84. <https://doi.org/10.3390/inorganics12030084>

Academic Editor: Antonino Gulino

Received: 17 January 2024

Revised: 29 February 2024

Accepted: 4 March 2024

Published: 8 March 2024



Copyright: © 2024 by the authors. Licensee MDPI, Basel, Switzerland. This article is an open access article distributed under the terms and conditions of the Creative Commons Attribution (CC BY) license (<https://creativecommons.org/licenses/by/4.0/>).

1. Introduction

The increasing global energy demand, coupled with the surge in greenhouse gas emissions and environmental challenges exacerbated by ongoing climate changes, emphasizes a need to develop sustainable energy harvesting systems. Notably, the energy and waste management sectors collectively contribute a 76.5% share of the world’s annual greenhouse gas emissions, amounting to 36.6 billion tons of CO₂ equivalent [1]. In numerous municipal administrations, drinking water and wastewater facilities tend to be the primary consumers of energy, frequently constituting 30 to 40 percent of the overall energy consumption [2,3]. Nearly 35% of the typical U.S. municipal energy budgets have been attributed to energy usage by water and wastewater utilities [4]. This stark reality highlights the urgency for innovative solutions for addressing energy efficiency and exploring sustainable practices, not only for environmental reasons but also for optimizing fiscal resources within public administration.

Enhancing the water–energy connection in wastewater management requires innovative materials and devices to efficiently harvest and simultaneously store energy. Each year,

about 100 billion gallons of wastewater generated by society harbors a potential energy yield of approximately 3600 GWh [2,3]. This energy is mainly contained in organic matter, nutrients, and thermal heat. Given the current energy-intensive nature of wastewater treatment processes, there is a pressing need for advancements to use the energy within the wastewater to drive the generation, movement, and treatment of wastewater.

Conventional energy storage systems, such as capacitors and solid-state batteries like lead–acid batteries, heavily rely on pure chemicals. Shifting towards energy harvesting devices that leverage accessible wastewater and microorganisms could significantly enhance the sustainability of both the energy and water industries. Regardless of the device type, the micro/nano-structure design of electrodes plays a pivotal role in determining their performance. Ongoing investigations into novel carbonaceous materials, like carbon nanotubes, particularly those synthesized from commonly discarded materials, are shaping advancements in electrochemistry devices. For instance, supercapacitors utilizing nanocrystalline cellulose within amorphous carbon fibers have demonstrated remarkable specific capacitances, reaching up to 201 F/g at 5 mV/s, along with a power density of 51.4 Wh/kg at 18 kW/kg [5]. The performance of the supercapacitors can be improved by leveraging the exceptional properties of two-dimensional materials (e.g., graphene and hexagonal boron nitride), including large surface area (2630 m²/g) [6,7], high charge storage (550 Farads/g) [8], electrical conductivity (1738 S/m) [9] charge carrier concentration (1013 cm⁻² at STP), and Fermi velocity (106 ms⁻¹).

Graphene exhibits immense potential for diverse applications, showcasing its prowess in high-capacity, fast-charging supercapacitors [10,11], flexible, rollable, and transparent batteries [12], and other devices [13]. Notably, graphene's barrier properties play a vital role in enhancing the corrosion resistance of metal-based electrodes, offering applications in biotic and abiotic applications [14–16]. While conventional graphene synthesis methods involve chemicals that are highly corrosive, explosive, and toxic [17,18], the plasma exfoliation process employed in this study stands out for its ability to synthesize graphene without such precursors. This process utilizes a dielectric barrier discharge plasma system under near-ambient conditions, showcasing a sustainable approach to graphene production.

This study utilizes plasma-exfoliated graphene layers to create a high-performance biobattery/supercapacitor device. The 3D Gr/Ni electrode, fed with wastewater, outperforms traditional electrodes, exhibiting a 150-fold increase in electrochemical power output (2582 mW/m²) and a 48-fold higher current density (12 A/m²) compared to bare Ni. Advanced testing methods, including microscopy and electrochemical impedance spectroscopy, reveal exceptional pseudocapacitive behavior (19,400 F/m²) at the Gr/Ni/biofilm interfaces. Additional electrochemical tests demonstrate the capability to store 250 mAh energy over almost 100 consecutive cycles. Modifying the biobattery architecture showcases supercapacitor behavior in Gr/Ni electrodes with a stronger electrolyte and symmetric reactor design.

2. Results and Discussion

2.1. Facile Strategy for the Synthesis of a 3D Bioanode

Figure 1a depicts the process of incorporating plasma-exfoliated graphene into a 3D Ni foam electrode. Graphene was exfoliated from graphene oxide (GO) using a low-temperature plasma process. A dielectric barrier discharge system induced a negative self-bias on GO samples, breaking the bonds between oxygen and carbon atoms. Ion bombardment resulting from this process allowed dissociated oxygen species to combine and form oxygen molecules between the GO layers. Beyond 70 W RF power and 3 Torr gas pressure, the thermal expansion of oxygen molecules within the GO layers led to graphene exfoliation. The resulting graphene was mixed with acetylene black and PTFE binder, and the mixture was mechanically pressed onto one side of the Ni foam while leaving the other three sides unaltered.

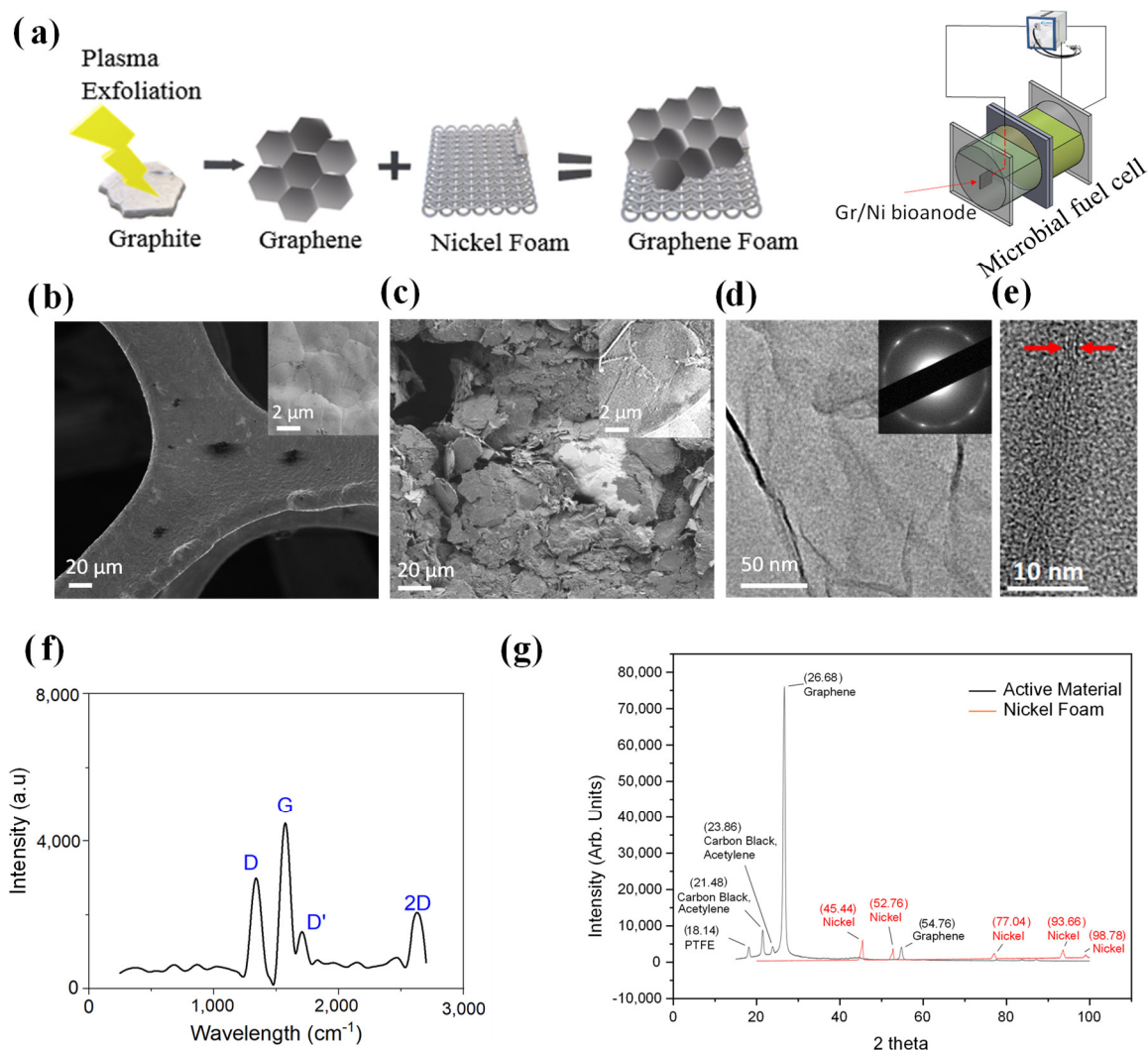


Figure 1. (a) Synthesis of Gr/Ni bioanode with low-temperature plasma exfoliation technique. SEM images of (b) bare Ni foam and (c) Gr/Ni bioanode. Inset shows higher magnification images of bare Ni foam and Gr/Ni foam (d). Transmission electron microscopy (TEM) image showing the sheets of graphene overlapped on each other and (e) folded edge showing three parallel lines, confirming the presence of three sheets of graphene. The inset in the image (d) shows a selected area electron diffraction pattern, confirming the crystalline and hexagonal nature of graphene. (f) Raman spectra of graphene. (g) XRD patterns for the active material with graphene and Ni foam. Active material represents graphene stacking.

2.2. Physical Characteristics of Bioanode

To assess the influence of Gr/Ni surface morphology on the hybrid biobattery-capacitor device's performance (discussed later), we conducted SEM image analysis on both unpressed and pressed sides of the Gr/Ni bioanode. The unpressed side without the active graphene mixture Figure 1b exhibited micron-scale pores conducive to nutrient delivery, bacterial colonization, and biofilm development. Figure 1d highlighted Ni grain boundaries, confirming the polycrystalline nature of Gr/Ni. On the pressed side Figure 1c, the graphene mixture formed a dense, stacked platelet structure, termed the "domino effect". This continuous bi-layered feature contributes to the capacitive properties of the Gr/Ni bioanode (discussed later). Figure 1e illustrates the even distribution of embedded Gr sheets within the active mixture matrix.

2.3. TEM, Raman and XRD Characterization

Transmission electron microscopy (TEM) analysis showed the transparent and crystalline structure of plasma-exfoliated graphene films on the copper grid Figure 1d. Both the dark gray areas and the folded edge, displaying three lines, suggest the presence of over three layers of stacked graphene sheets. The selected area diffraction pattern affirmed the hexagonal nature of graphene, supporting the presence of at least two layers of Gr sheets Figure 1d. This result emphasizes that fewer folds in the graphene sheet enhance the accessible surface area for microbial attachment [19].

Figure 1f displays the Raman spectrum of Gr/Ni samples corresponding to Figure 1. The datasets underwent smoothing using the Savitzky–Golay fitting method. The D peak indicates defects in the graphene sheets, and the D' peak signifies the double resonance of an intravalley process. The Raman spectrum exhibits two prominent peaks: the G peak at 1572 cm^{-1} and the 2D peak at 2698 cm^{-1} , both confirming the presence of graphene. The ratio of the intensity of the G and 2D peaks ($I_G/I_{2D} \approx 2$) suggests the existence of multilayered graphene.

Figure 1g presents the XRD patterns recorded for the active material with graphene and Ni foam in a 2θ range of 15° to 100° . Graphene displays a (002) diffraction peak at 26.68° , indicating an interlayer spacing of 3.34 \AA between graphene sheets, calculated by Bragg's law [15]. This suggests that the graphene sheets are stacked within the active material, resulting in the diffraction peak at 26.68° . Ni exhibits sharp diffraction peaks at 45.44° , 52.76° , 77.04° , 93.66° , and 98.78° corresponding to the (111), (200), (220), (311), and (222) Ni planes, confirming the polycrystalline nature of the Ni foam [20]. The diffraction peaks of PTFE and carbon black are identified at 18.14° and 23.86° , respectively [21].

2.4. Exceptional Electrochemical Power Output

Figure 1e illustrates the working principles of a biobattery. The initial microbial population included bacteria from the genus classes of *Corynebacterium* (34.3%), *Bacteroides* (16.6%), *Shewanella* (11.34%), *Ruminobacillus* (8.28%), and other miscellaneous species (29.48%). In biobatteries, the electroactive biofilm formed on the Gr/Ni anode surface facilitates the bioelectrochemical oxidation of acetate-supplemented wastewater. A significant finding is the Gr/Ni bioanode's exceptional electrochemical power output compared to controls (bare Ni and graphite felt) under identical biobattery conditions. The peak open-circuit voltage for Gr/Ni (0.58 V) was 69% higher than the Ni foam (0.18 V) and equivalent to graphite felt (0.62 V). The peak power density for the Gr/Ni bioanode (2582 mW/m^2) was 152-fold and 4-fold higher compared to bare Ni (16.9 mW/m^2) and graphite felt (650 mW/m^2). The peak current density for Gr/Ni bioanode ($12,000\text{ mA/m}^2$) was 48-fold and 3-fold higher compared to bare Ni (250 mA/m^2) and graphite felt (3850 mA/m^2), respectively.

Furthermore, the power output of Gr/Ni bioanode (2582 mW/m^2) surpasses commercial electrodes, including graphite felt and RVC, as well as those based on graphene. For instance, the current density of the Gr/Ni bioanode (13 A/m^2) is larger than prior studies based on graphene sponge in a mixed microbial culture system [22] and CVD-based graphene (*Shewanella oneidensis* MR-1 system) [23].

Gr/Ni bioanode exhibited a well-defined polarization response (a characteristic bell curve) and maintained high electrochemical power output and current densities throughout the 65 days of the experimental duration (Figure 2a), even after media replacements. The Gr/Ni bioanode demonstrated a dominant polarization response and enhanced power density curves from day 16 until day 65. For instance, the peak power density values for the Gr/Ni bioanode on day 7 (initial performance), day 16 (after biofilm formation), and day 65 (steady-state performance) were 7.3 mW/m^2 , 2582 mW/m^2 , and 2289 mW/m^2 , respectively. This distinctive bell curve was not observed in the Ni control Figure 2b. The performance of biobatteries with bare Ni foam diminished within seven days of operation (Figure 2). The Ni foam impregnated with acetylene black and PTFE (lacking graphene) did not replicate the exceptional performance of the Gr/Ni bioanode (results not shown).

These results confirm that the enhanced performance of the Gr/Ni bioanode is attributed to the presence of plasma-exfoliated graphene nanosheets.

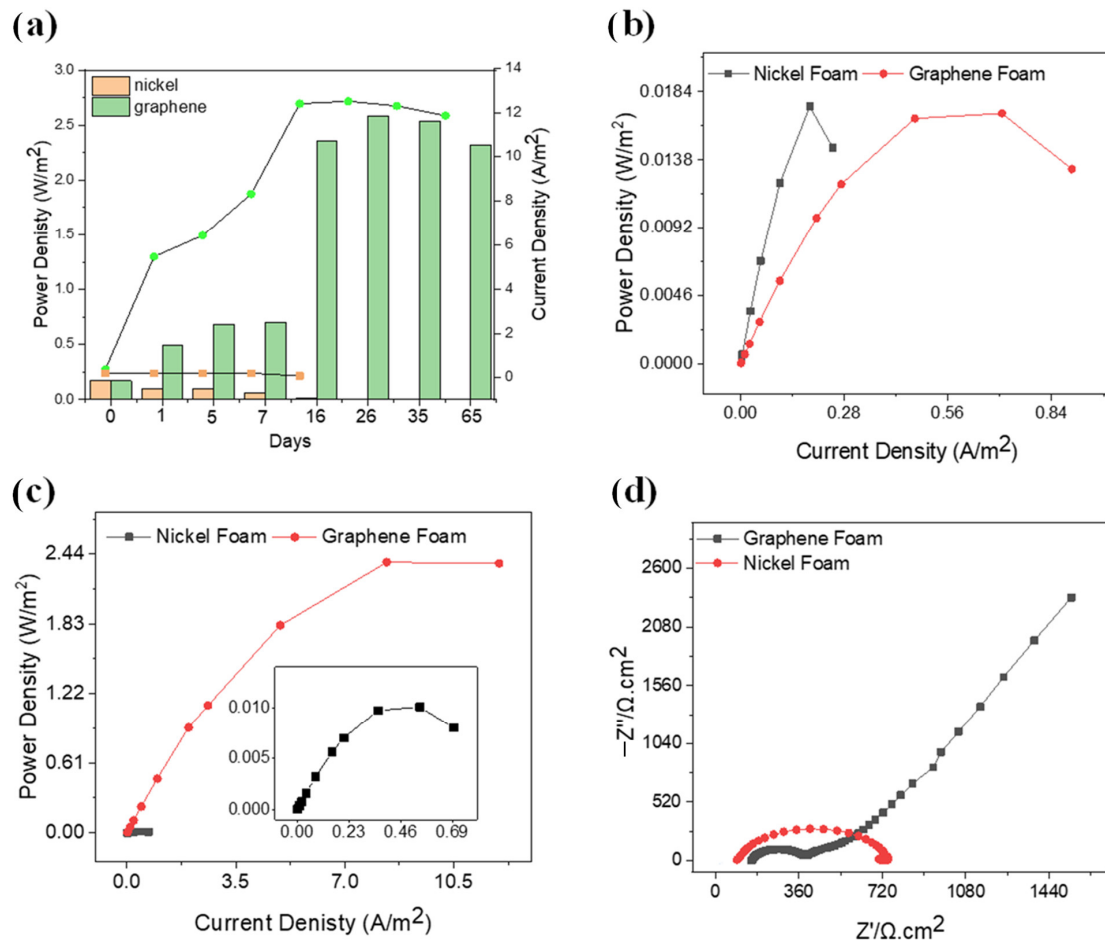


Figure 2. (a) Power density and current density of the Gr/Ni and Ni bioanode over time (day). (b) Ni and Gr/Ni data, and all remaining Ni data are multiplied by 10 to fit in the plot. (c) Temporal power curves with enlarged Ni plots. (d) Full-cell EIS configuration for different electrodes (Gr/Ni and Ni).

The EIS analysis results confirm that the superior electrochemical performance of the device is attributed to its ability to lower the overall impedance compared to controls (bare Ni and graphite felt) (Figures 3b and 4). According to the external equivalent circuit (EEC) fitting analysis, the overall impedance of the Gr/Ni biobattery ($2580 \Omega \text{ cm}^2$) was 27-fold and 4-fold lower than Ni foam ($93.9 \Omega \text{ cm}^2$) and graphite felt ($375.5 \Omega \text{ cm}^2$), respectively. Notably, the charge transfer resistance of the Gr/Ni bioanode ($0.1 \Omega \text{ cm}^2$) was 2153-fold and 61-fold lower than Ni foam ($215.3 \Omega \text{ cm}^2$) and graphite felt ($6.1 \Omega \text{ cm}^2$), respectively.

The enhanced performance of Gr/Ni bioanodes is attributed to their superior properties related to the accessible surface area, electrical conductivity, and electrochemical stability. SEM tests revealed that the pressed side of the Gr/Ni foam (facing the membrane) was entirely covered with a highly conductive graphene mixture (Figure 1a), enhancing electrical communication between the cells and the electrode. This conclusion is supported by the thicker biofilms observed on the Gr/Ni bioanodes (Figure 2). The pressed side (treated with graphene) of the Gr/Ni bioanode (facing the membrane) is characterized by higher values of electrical conductivity and accessible surface area, promoting electronic communication between the electroactive microbes and the Gr/Ni bioanode. The unpressed sides, characterized by micron-scale pore structures, enable unimpeded nutrient delivery, initial bacterial attachment, and subsequent biofilm development. However, as discussed in subsequent sections, electrode properties alone do not entirely explain the

basis for the higher power output of the device. This performance improvement is also due to the capacitive behavior of the Gr/Ni bioanode.

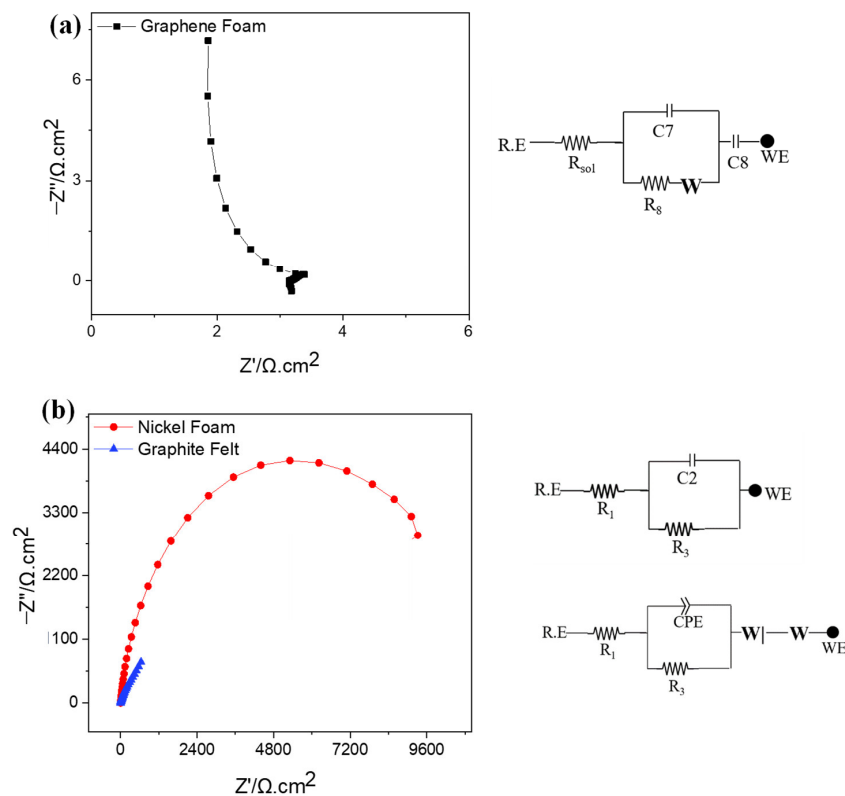


Figure 3. Nyquist curves and its corresponding electrical equivalent circuit for: (a) Gr/Ni bioanode, (b) bare Ni bioanode.

The literature presents varying findings regarding the antimicrobial properties of graphene materials. For example, certain studies have suggested antimicrobial properties of graphene coatings against bacteria like *E. coli* and *B. subtilis* [24], while research by Novoselov and colleagues has shown that graphene materials neither stimulate nor inhibit the growth of these bacteria [25,26]. These variations in the antimicrobial performance of graphene materials can be attributed to the nature of the synthesis methods. For example, wet chemistry methods have a higher tendency to introduce impurities originating from toxic precursors (e.g., hydrazine for synthesizing graphene from graphite oxide) [27]. However, chemical vapor deposition (CVD) methods do not induce any such chemical impurities in the resulting graphene materials. Our own studies have demonstrated that the CVD-based graphene materials on metal substrates neither restrict cell attachment nor biofilm growth of micro-organisms such as sulfate-reducing bacteria [15,16]. Additionally, our recent studies have shown that graphene materials based on CVD [28] and plasma exfoliation (the method used in this study) provide conducive environments for promoting cell attachment and growth of biofilms based on methylotrophs in microbial fuel cell applications. Similarly, a study by Wang et al. also suggests that 3D graphene–nickel foam electrodes offer a high volumetric power density of 661 W/m^3 in microbial fuel cells, which typically rely upon biofilm growth [29]. Another study using a graphene composite-based nickel foam anode reported a power density of 18.8 W/m^3 [30]. Zhang et al. also used a nickel foam/graphene composite electrode and reported enhanced power generation (36.4 mW/m^2) [31]. Not only has graphene–nickel been used in anodes, but it has also been used in cathode materials. Song et al. concluded that using a 3D graphene–nickel foam as a cathode improved bacterial colonization and the efficiency of microbial electrosynthesis of acetate from carbon dioxide [32].

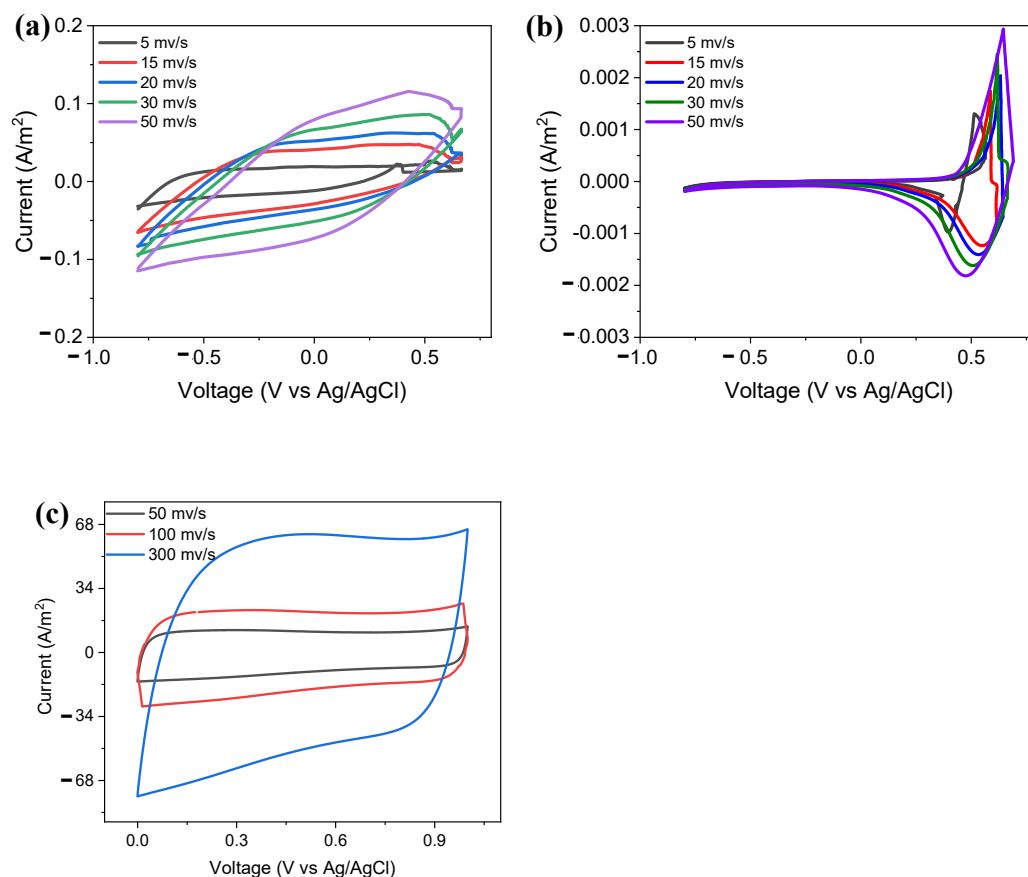


Figure 4. CV plots show capacitive behavior at different scan rates for (a) Gr/Ni foam abiotic KOH solution; (b) Gr/Ni bioanode biotic mixed culture; (c) Ni foam biotic mixed culture.

2.5. A Unique Impedance Signature of Capacitive Behavior

A unique finding in this study is the Gr/Ni/biofilm interface's ability to capacitively store charges within the biobattery architecture using biological media (weak electrolyte). The interface facilitates both the adsorption/desorption of ions (electrochemical double-layer charging) and the storage of charges from typical Faradaic reactions associated with the bio-electrochemical oxidation of acetate-supplemented wastewater (pseudocapacitance). The Nyquist curve for the Gr/Ni bioanode exhibits a quasi-semicircle (100 kHz to 0.16 Hz), followed by a diffusion impedance tail that abruptly reverses direction, turning into a vertical sloping line in the low-frequency region (0.06 to 0.01 Hz) (Figure 4a). This impedance behavior is typically observed in energy-harvesting devices, such as supercapacitors [33]. In this context, the quasi-semicircle represents impedance to ionic species diffusing into the electrical double-layer capacitance layer, while the tail implies Warburg impedance. The persistent presence of the semicircle–diffusion–tail behavior throughout the 70 days of the biobattery tests suggests the capacitive behavior of the Gr/Ni bioanode.

The absence of a semicircle-sloping Nyquist spectrum in the bioanode based on bare Ni foam further confirms that the capacitive behavior observed in Gr/Ni is not due to interference caused by the adsorption of biological components. The Nyquist curves for the controls (bare Ni and graphite felt bioanode) display a perfect semicircle in high-to-low-frequency regions, representing impedance to charge transfer reactions associated with bio electrochemical oxidation of acetate-supplemented wastewater (Figure 3b). Typical bioanode materials (e.g., RVC, carbon brush, and metal foams) exhibit Nyquist spectra characterized by an arc shape at the high-frequency region (activation-controlled charge transfer reaction) followed by a beeline in the low-frequency region (diffusion-controlled charge transfer reaction). Finally, quantitative confirmation of the capacitive behavior of Gr/Ni bioanode was achieved through equivalent circuit fitting analysis. The specific ca-

capitance at the Gr/Ni bioanode EDLC interface (1.9 F/cm^2) was 100-fold higher compared to the controls (0.02 F/cm^2). The hierarchical pore structure of Gr/Ni provides adequate accessible pathways for high-rate ion diffusion and subsequent capacitive behavior [34].

2.6. Cyclic Voltammetry Confirms Capacitive Properties of Gr/Ni Bioanode

The cyclic voltammogram of the Gr/Ni bioanode exhibits characteristics of electric double-layer capacitance, providing further evidence of the capacitive nature observed in Gr/Ni electrodes from the EIS results. The Gr/Ni bioanodes display a quasi-rectangular voltammogram, emphasizing their pseudocapacitive nature (Figure 5). To evaluate the capacitive behavior of the Gr/Ni foam under optimal conditions, CV tests were repeated using a strong KOH electrolyte and a symmetric cell modeled by a 2032 coin cell. The Gr/Ni electrode produced a perfectly rectangular voltammogram with strong electrochemical reversibility, highlighting the supercapacitor nature of the Gr/Ni electrode (Figure 4a). The voltammogram of the Gr/Ni electrode in both biotic and abiotic conditions exhibits capacitive behavior, while the Ni foam displays distinct anodic and cathodic plots [35]. With increasing scan rate, the CV plots for Gr/Ni show a broader current response with no distinct redox peaks (Figure 4a), whereas the Ni foam exhibits distinct anodic and cathodic peaks for redox reactions between 0.25 V and 0.75 V (Figure 4b). The peak value of the current density in the CV plot for the Gr/Ni electrode in biological media (0.14 A/m^2) and KOH electrolyte (62 A/m^2) is 78-fold and 34,500-fold higher compared to the Ni foam (0.0018 A/m^2).

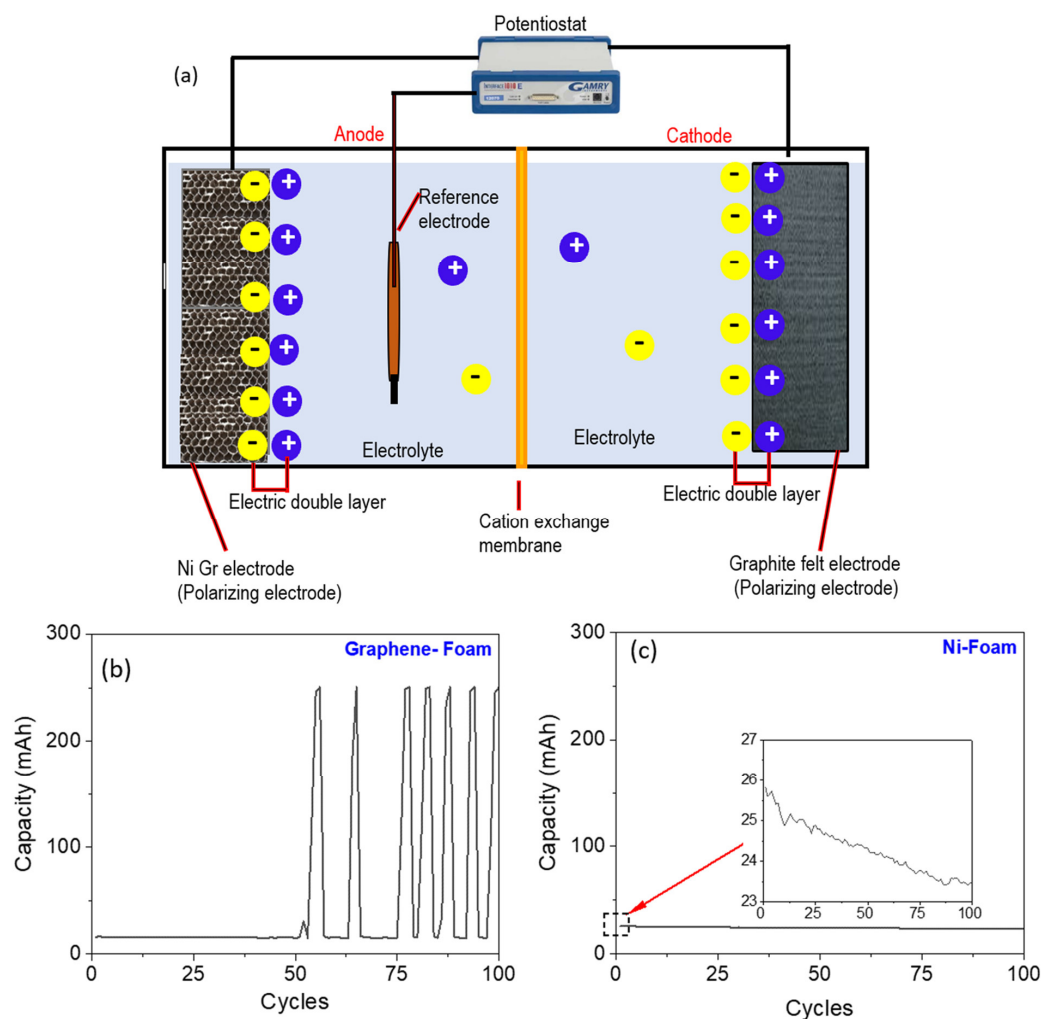


Figure 5. (a) Schematic of pseudocapacitive behavior of Gr/Ni bioanode-based microbial fuel cell. Charge/discharge cycles, (b) graphene/nickel foam, (c) bare Ni foam.

2.7. Charge/Discharge Properties of Gr/Ni Bioanode

To evaluate the charge storage capacity of the electric double-layer capacitor on the Gr/Ni/ interface, rapid charge and discharge tests were conducted using Gr/Ni as the working electrode and graphite felt as the counter electrode. The tests utilized the spent anolyte from day 65 as the electrolyte, comprising planktonic cells, and typical charged species (Na^+ , CH_3COO^- , Fe^{3+} , K^+ , $\text{Fe}(\text{CN})_6^{3-}$, and Ni^{2+}) that constituted the source of charges in the EDLC at the Gr/Ni/anolyte interfaces. Considering the use of a proton exchange membrane in the biobattery architecture, the diffusion of ions into the cathode compartment can be expected. Figure 5a presents a hypothetical schematic illustrating the potential Faradaic and non-Faradaic reactions contributing to the capacitive behavior of the Gr/Ni/biofilm interface. The schematic in Figure 5a depicts the formation of the EDLC next to the Gr/Ni bioanode, demonstrating the diffusion path and charge transfer mechanism. Impedance increases with longer diffusion paths in the electrolyte, and changes in the concentration of the electrolyte affect the charge transfer reaction, altering the ratio between the given overpotential and the subsequent Faradaic current [36].

In Figure 5b, the results from 100 rapid and consecutive charging and galvanostatic discharging tests are presented. Over the initial 50 cycles, Gr/Ni yielded 18mAh, later peaking at 250 mAh. The charge storage capacity of the Gr/Ni bioanode peaked at 250 mAh, representing a tenfold increase compared to the Ni bioanode (24 mAh). Additionally, while the Ni foam experienced declining capacitance over time, Gr/Ni consistently delivered 250 mAh for the last 50 cycles. The identical biobattery architecture for both Gr/Ni and Ni bioanodes further supports the graphene mixture's role in the capacitive behavior and associated increase in electrochemical power output.

3. Experimental Section

3.1. Source of Wastewater

The municipal wastewater used in this study was collected from the primary clarifier effluent of Rapid City's Wastewater Reclamation Facility (WRF). Rapid City's WRF system provides service for residential, commercial, and current industrial customers in Rapid City and for several regional customers. The wastewater collection phase involves collecting water from the primary clarifier, strategically located after the grit removal tank, where large debris is effectively removed. Notably, up to this point in the WRF system, there is no biological oxygen demand (BOD) removal, ensuring the retention of nutrients essential for subsequent biofilm formation. This pragmatic approach emphasizes the role of the primary clarifier in facilitating efficient downstream biological processes within the wastewater treatment system.

3.2. Graphene Exfoliation with Low-Temperature Discharge Plasma

We employed a dielectric barrier discharge plasma system for exfoliating graphene sheets from graphene oxide (GO), following the procedures outlined by [10]. The plasma system utilized a quartz tube equipped with a vacuum pump, gas flow controller, and a 13.56 MHz radio frequency (RF) power supply with a matching network. The process involved placing 300 mg of GO in the quartz tube, followed by three cycles of evacuation and purging with N_2 gas to eliminate residual air. Maintaining a stable pressure of 28 m Torr in the chamber, the RF power was manually switched on, and the matching network was tuned to achieve zero-watt reflection power. Graphene exfoliation was accomplished by adjusting the chamber pressure to 3 Torr and increasing the RF power to 70 W. Following successful exfoliation, the RF power, gas flow, and vacuum pump were sequentially switched off to vent the chamber. Graphite oxide was synthesized using the modified Hummer method, as detailed in our earlier work [16].

3.3. Fabrication of Graphene Electrodes

To create 3D Gr/Ni electrodes, a graphene mixture was formed by combining 80 wt% plasma-exfoliated graphene, 10 wt% acetylene black (to improve the conductivity) and

10 wt% PTFE (to serve as binder). This mixture was mechanically pressed onto one side of Ni foam (1 in × 1 in) (EQ-bcnf-16m, MTI Corp) at 1000 kg/cm² pressure for 10 min. The treated electrodes were dried at 60 °C for 12 h, and the Gr/Ni electrodes served as working electrodes in both biobattery and supercapacitor devices. Controls included bare Ni foam and Ni foam with 10 wt% acetylene black and 10 wt% PTFE.

3.4. A Hybrid Battery–Supercapacitor Device

We designed a biobattery employing a two-compartment microbial fuel cell configuration utilizing wastewater as an electrolyte, electroactive microorganisms as biocatalysts, and a 100 mM ferricyanide solution as the catholyte. The biobatteries were configured using a two-compartment fuel cell configuration and operated at 25 °C under a fed-batch mode, following the protocols outlined in our previous studies [15,37]. The anode and cathode compartments in the biobattery had a volumetric capacity of 15 mL each. Test biobatteries utilized Gr/Ni as the working electrode, while controls employed bare Ni, bare Ni with PTFE, acetylene black, and graphite felt (See Table 1 for nomenclature). The anolyte composition comprised 12.5 mL of primary clarifier effluent, 2.5 mL of effluent from an active microbial fuel cell with a one-year operating history, and supplements based on 100 mM sodium acetate, 0.4 g/L of BES, 1.25% minerals, and 0.5% vitamins. Initial anolyte values included a pH of 7 ± 0.5 and a chemical oxygen demand (COD) of 6610 mg/L. The fed-batch performance of both test and control biobatteries was continuously monitored over a 72-day period (Table 2).

Table 1. Comparison of Gr/Ni studies from the existing literature.

Materials Used	Graphene Deposition Method	OCV (V)	Power Density (mW/m ²)	Current Density (A/m ²)	Inoculum	Ohmic Loss (Ω)	Reference
Graphene	Plasma deposition	0.65	2582	12.9	Wastewater	28	This study
Graphene oxide	Autoclaved and annealed	0.62	721	1.76	<i>Shewanella oneidensis</i> MR-1	10	[19]
3D graphene	Chemical vapor deposition	n/a	768	1.8	<i>Shewanella oneidensis</i> MR-1	9	[23]
Graphene sponge	Chemical vapor deposition	0.33	1110	1.32	Wastewater	14	[22]

Table 2. Experimental details for biobattery and capacitor tests.

Test	#	Reactor	Working Electrode	Test	Electrolyte	Purpose
Biotic (65 days)	Graphene on nickel foam (referred to as graphene foam)	Biobattery	Gr/Ni (or Graphene Foam)	EIS, CV	Wastewater anolyte	Measure current, power output, and biofilm growth
	3D nickel foam	Biobattery	Bare Ni (or Ni foam)	EIS, CV	Wastewater anolyte	Control
	Graphite felt	Biobattery	Graphite felt	EIS	Wastewater anolyte	Control for EIS studies
	3D graphene	Capacitor	Gr/Ni	Charging/discharging cycle	Wastewater anolyte	Establish charge storage properties of graphene foam
Abiotic	3D Ni	Capacitor	Bare Ni	Charging/discharging	Wastewater anolyte	Control
	Coin cell	Super Capacitor	Gr/Ni	CV	KOH (anolyte and catholyte)	Establish bifunctional device

3.5. Charging/Discharging Cycles and Capacitive Behavior of the Device

Post-day 65, the capacitive characteristics of the Gr/Ni bioanode, including the pre-formed biofilm, were evaluated through cyclic voltammetry (CV) and charge/discharge cycle tests. The Gr/Ni/biofilm served as the working electrode, with the cathode as the counter electrode and Ag/AgCl as the reference electrode. The spent anolyte from the biobattery acted as the electrolyte for the capacitor tests. Charge and discharge capabilities were examined over nearly 100 cycles, with a maximum charge time of 30 s at a 5 mA charging current. Following charging, a 10 s stabilization period preceded a 30 s discharge using a constant load of 33 Ω . In additional abiotic experiments, capacitive properties of the Gr/Ni electrode (1 cm²) were assessed using a 2032 stainless-steel coin cell with a microporous polypropylene separator and 6 mol L⁻¹ KOH.

3.6. Surface Analysis and Chemical Composition

Following the biobattery-supercapacitor tests, post-mortem analysis was conducted on the Ni and Gr/Ni bioanodes to examine biofilm formation. For SEM analysis, samples were rinsed with 0.1 M PBS (pH 7.2) and treated with 2% glutaraldehyde in 0.1 M PBS for 24 h at room temperature [38,39]. After rinsing with PBS and distilled water, samples were dehydrated with ethanol solutions (35%, 50%, 80%, 90%, and 100% *v/v*) and dried overnight in a desiccator. A Zeiss Supra40 variable-pressure field-emission SEM (Carl Zeiss SMT AG Company, Oberkochen, Germany) with an Oxford Aztec Energy system (software version 5.1) was used for morphological and chemical analysis. The SEM was operated at 5 kV for image analysis and 15 kV for elemental analysis. Raman spectra of the Ni and Gr/Ni foam samples were recorded using ffTA Foram X3 module (Foster + Freeman Ltd., Evesham, UK) with a 532 nm excitation source. Chemical composition analysis of the biofilm utilized a Rigaku Ultima-Plus XRD (Malvern Panalytical Inc., Westborough, MA, USA) configured with CuK α radiation. Samples were scanned from 10° to 80° at a rate of 2° 2 θ /min. TEM images and selected area electron diffraction patterns were obtained using a JEM-2100 LaB6 TEM (Jeol USA Inc., Peabody, MA, USA).

3.7. Analytical Methods

Electrolyte pH was measured using an Orion Star log R pH benchtop and soluble COD was determined through standard 5220 methods [21]. The polarity of the biobatteries and the integrity of the resistance boxes simulating external loads were verified using a commercial voltmeter.

3.8. Electrochemical Methods

Voltage data were collected using a DAQ/54 module (I/O Tech Inc., Cleveland, OH, USA) across an external load. Electrochemical impedance spectroscopy (EIS) tests were conducted with a Gamry reference 3000 electrochemical workstation. EIS profiles for the electrodes were acquired for both anode and full-cell configurations, with the initial frequency set at 100 KHz and the final frequency completed at 10 mHz. The DC voltage for EIS and cyclic voltammetry (CV) tests was obtained against an Ag/AgCl reference electrode. Cyclic voltammetry was carried out at a scan rate of 5 to 50 mV/s and within the range of -1 to 1 V.

4. Outlook

Our previous investigations utilizing a comparable biobattery device, designed similar to a two-compartment MFC, already demonstrated COD removal rates ranging from 75% to 94% using the same municipal wastewater [40] employed in the present study. Building upon these findings, it is evident that hybrid biobattery devices hold potential for harnessing and storing energy that can be utilized for enhancing the sustainability of secondary and tertiary treatment processes. The energy harvested by the biobattery device can power the pumps needed for a standard ultrafiltration module intended for wastewater reuse. It can also partially or entirely fulfill the electricity needs of various equipment

commonly employed in wastewater treatment processes. These include pumps, motors for screens, grit chambers, skimmers, and sludge rakes, as well as compressors or aerators. Additionally, it can power lamps used for UV disinfection, motors for mixing and filter presses in sludge treatment, and HVAC and lighting systems in buildings and surrounding areas [41].

Global sanitation faces challenges due to the energy-intensive nature of wastewater treatment. Embracing energy recovery technologies can enhance accessibility, particularly in economically disadvantaged areas. While MFC systems show promise for wastewater treatment, issues including high costs, especially for energy harvesting and storage, hinder widespread use. Our study of graphene on nickel materials, demonstrating promising results with exceptional charge storage capacity (19,400 F/m²), opens avenues for developing nickel-containing metals (e.g., steel) as inexpensive electrodes for electricity generation from wastewater and simultaneous storage, offering environmental friendliness, ease of production, and practical scalability for kilowatt-level power. The viability of such electrodes can be greatly improved by utilizing low-value materials (such as asphaltene and solid wastes) as graphene precursors and leveraging waste heat to accelerate wastewater oxidation kinetics.

5. Conclusions

In remote regions of certain developing nations, millions of people are projected to lack electricity in the coming years. Combining the increasing challenges of sanitation and wastewater management, the development of a hybrid biobattery–supercapacitor emerges as an attractive solution. The capacitive graphene electrodes showcased superior electrochemical performance (2.58 W/m², 12 A/m²) and capacitive behavior (250 mAh, 50 cycles). Further optimization of materials and engineering parameters holds the potential to enhance the energy density of these electrodes. Further studies are needed to address factors like wastewater chemistry, electrode longevity, and facility diversity for optimizing hybrid biobatteries for specific real-world operations.

Author Contributions: Conceptualization, V.G. and Z.G.; methodology, S.S.; software, S.S., N.S. and S.P.K.; validation, V.G., Z.G. and N.S.; formal analysis, S.S. and N.S.; investigation, S.S. and N.S.; resources, J.B. and M.Z.; data curation, S.S., S.P.K. and M.H.; writing—original draft preparation, S.S.; writing—review and editing, V.G., Z.G., M.Z. and J.B.; visualization, V.G.; supervision, V.G. and Z.G.; project administration, V.G.; funding acquisition, V.G. All authors have read and agreed to the published version of the manuscript.

Funding: This research was funded by NASA (NNX16AQ98A) and the National Science Foundation CAREER Award (#1454102).

Data Availability Statement: The data presented in this study are available in article.

Conflicts of Interest: The authors declare no conflict of interest.

References

1. Bhatt, R.P. Achievement of SDGS globally in biodiversity conservation and reduction of greenhouse gas emissions by using green energy and maintaining forest cover. *GSC Adv. Res. Rev.* **2023**, *17*, 001–021. [CrossRef]
2. Environmental Protection Agency. Energy Efficiency for Water Utilities. Available online: <https://www.epa.gov/sustainable-water-infrastructure/energy-efficiency-water-utilities> (accessed on 25 October 2023).
3. Environmental Protection Agency. Global Greenhouse Gas Emissions Data. Available online: <https://www.epa.gov/ghgemissions/global-greenhouse-gas-emissions-data> (accessed on 15 January 2024).
4. Malcolm Pirnie, Inc.; New York State Energy Research and Development Authority. *Statewide Assessment of Energy Use by the Municipal Water and Wastewater Sector: Final Report*; New York State Energy Research and Development Authority: Albany, NY, USA, 2008.
5. Sayed, D.M.; El-Deab, M.S.; Elshakre, M.E.; Allam, N.K. Nanocrystalline cellulose confined in amorphous carbon fibers as capacitor material for efficient energy storage. *J. Phys. Chem. C* **2020**, *124*, 7007–7015. [CrossRef]
6. Wang, K.; Xu, M.; Gu, Y.; Gu, Z.; Liu, J.; Fan, Q.H. Low-temperature plasma exfoliated n-doped graphene for symmetrical electrode supercapacitors. *Nano Energy* **2017**, *31*, 486–494. [CrossRef]

7. Pumera, M. Electrochemistry of graphene: New horizons for sensing and energy storage. *Chem. Rec.* **2009**, *9*, 211–223. [[CrossRef](#)] [[PubMed](#)]
8. Wong, S.I.; Sunarso, J.; Wong, B.T.; Lin, H.; Yu, A.; Jia, B. Towards enhanced energy density of graphene-based supercapacitors: Current status, approaches, and future directions. *J. Power Sources* **2018**, *396*, 182–206. [[CrossRef](#)]
9. Yu, M.; Feng, X. Thin-film electrode-based supercapacitors. *Joule* **2019**, *3*, 338–360. [[CrossRef](#)]
10. Huang, Y.; Sutter, E.; Shi, N.N.; Zheng, J.; Yang, T.; Englund, D.; Gao, H.-J.; Sutter, P. Reliable exfoliation of large-area high-quality flakes of graphene and other two-dimensional materials. *ACS Nano* **2015**, *9*, 10612–10620. [[CrossRef](#)] [[PubMed](#)]
11. Yu, M.; Peng, Y.; Wang, X.; Ran, F. Emerging Design Strategies Toward Developing Next-Generation Implantable Batteries and Supercapacitors. *Adv. Funct. Mater.* **2023**, *33*, 2301877. [[CrossRef](#)]
12. Naebe, M.; Wang, J.; Amini, A.; Khayyam, H.; Hameed, N.; Li, L.H.; Chen, Y.; Fox, B. Mechanical property and structure of covalent functionalised graphene/epoxy nanocomposites. *Sci. Rep.* **2014**, *4*, 4375. [[CrossRef](#)]
13. Ferrari, A.C.; Basko, D.M. Raman spectroscopy as a versatile tool for studying the properties of graphene. *Nat. Nanotechnol.* **2013**, *8*, 235–246. [[CrossRef](#)]
14. Chilkoor, G.; Sarder, R.; Islam, J.; ArunKumar, K.; Ratnayake, I.; Star, S.; Jasthi, B.K.; Sereda, G.; Koratkar, N.; Meyyappan, M. Maleic anhydride-functionalized graphene nanofillers render epoxy coatings highly resistant to corrosion and microbial attack. *Carbon* **2019**, *159*, 586–597. [[CrossRef](#)]
15. Chilkoor, G.; Shrestha, N.; Kutana, A.; Tripathi, M.; Herna, F.C.R.; Jakobson, B.I.; Meyyappan, M.; Dalton, A.B.; Ajayan, P.M.; Rahman, M.M. Atomic layers of graphene for microbial corrosion prevention. *ACS Nano* **2020**, *15*, 447–454. [[CrossRef](#)]
16. Krishnamurthy, A.; Gadhamshetty, V.; Mukherjee, R.; Chen, Z.; Ren, W.; Cheng, H.-M.; Koratkar, N. Passivation of microbial corrosion using a graphene coating. *Carbon* **2013**, *56*, 45–49. [[CrossRef](#)]
17. Anagbonu, P.; Ghali, M.; Allam, A. Low-temperature green synthesis of few-layered graphene sheets from pomegranate peels for supercapacitor applications. *Sci. Rep.* **2023**, *13*, 15627. [[CrossRef](#)]
18. Kulyk, B.; Freitas, M.A.; Santos, N.F.; Mohseni, F.; Carvalho, A.F.; Yasakau, K.; Fernandes, A.J.S.; Bernardes, A.; Figueiredo, B.; Silva, R. A critical review on the production and application of graphene and graphene-based materials in anti-corrosion coatings. *Crit. Rev. Solid State Mater. Sci.* **2022**, *47*, 309–355. [[CrossRef](#)]
19. Wang, Y.; Li, Y.; Tang, L.; Lu, J.; Li, J. Application of graphene-modified electrode for selective detection of dopamine. *Electrochem. Commun.* **2009**, *11*, 889–892. [[CrossRef](#)]
20. Prina-Mello, A.; Diao, Z.; Coey, J. Internalization of ferromagnetic nanowires by different living cells. *J. Nanobiotechnol.* **2006**, *4*, 9. [[CrossRef](#)]
21. Tian, Z.Q.; Wang, X.L.; Zhang, H.M.; Yi, B.L.; Jiang, S.P. Microwave-assisted synthesis of PTFE/C nanocomposite for polymer electrolyte fuel cells. *Electrochem. Commun.* **2006**, *8*, 1158–1162. [[CrossRef](#)]
22. Xie, X.; Yu, G.; Liu, N.; Bao, Z.; Criddle, C.S.; Cui, Y. Graphene-sponges as high-performance low-cost anodes for microbial fuel cells. *Energy Environ. Sci.* **2012**, *5*, 6862–6866. [[CrossRef](#)]
23. Yong, Y.-C.; Dong, X.-C.; Chan-Park, M.B.; Song, H.; Chen, P. Macroporous and monolithic anode based on polyaniline hybridized three-dimensional graphene for high-performance microbial fuel cells. *ACS Nano* **2012**, *6*, 2394–2400. [[CrossRef](#)] [[PubMed](#)]
24. Santos, C.M.; Mangadla, J.; Ahmed, F.; Leon, A.; Advincula, R.C.; Rodrigues, D.F. Graphene nanocomposite for biomedical applications: Fabrication, antimicrobial and cytotoxic investigations. *Nanotechnology* **2012**, *23*, 395101. [[CrossRef](#)] [[PubMed](#)]
25. Sasidharan, A.; Panchakarla, L.S.; Chandran, P.; Menon, D.; Nair, S.; Rao, C.N.R.; Koyakutty, M. Differential nano-bio interactions and toxicity effects of pristine versus functionalized graphene. *Nanoscale* **2011**, *3*, 2461–2464. [[CrossRef](#)]
26. Barbolina, I.; Woods, C.R.; Lozano, N.; Kostarelos, K.; Novoselov, K.S.; Roberts, I.S. Purity of graphene oxide determines its antibacterial activity. *2D Materials* **2016**, *3*, 025025. [[CrossRef](#)]
27. Lin, H.; Buerki-Thurnherr, T.; Kaur, J.; Wick, P.; Pelin, M.; Tubaro, A.; Carniel, F.C.; Tretsch, M.; Flahaut, E.; Iglesias, D.; et al. Environmental and Health Impacts of Graphene and other Two-Dimensional Materials: A Graphene Flagship Perspective. *ACS Nano* **2024**, *18*, 6038–6094. [[CrossRef](#)]
28. Islam, J.; Obulisamy, P.K.; Upadhyayula, V.K.; Dalton, A.B.; Ajayan, P.M.; Rahman, M.M.; Tripathi, M.; Sani, R.K.; Gadhamshetty, V. Graphene as Thinnest Coating on Copper Electrodes in Microbial Methanol Fuel Cells. *ACS Nano* **2022**, *17*, 137–145. [[CrossRef](#)] [[PubMed](#)]
29. Wang, H.; Wang, G.; Ling, Y.; Qian, F.; Song, Y.; Lu, X.; Chen, S.; Tong, Y.; Li, Y. High power density microbial fuel cell with flexible 3D graphene-nickel foam as anode. *Nanoscale* **2013**, *5*, 10283–10290. [[CrossRef](#)]
30. Karthikeyan, R.; Krishnaraj, N.; Selvam, A.; Wong, J.W.-C.; Lee, P.K.; Leung, M.K.; Berchmans, S. Effect of composites based nickel foam anode in microbial fuel cell using *Acetobacter acetii* and *Gluconobacter roseus* as biocatalysts. *Bioresour. Technol.* **2016**, *217*, 113–120. [[CrossRef](#)]
31. Zhang, Y.; He, Q.; Xia, L.; Li, Y.; Song, S. Algae cathode microbial fuel cells for cadmium removal with simultaneous electricity production using nickel foam/graphene electrode. *Biochem. Eng. J.* **2018**, *138*, 179–187. [[CrossRef](#)]
32. Song, T.; Fei, K.; Zhang, H.; Yuan, H.; Yang, Y.; Ouyang, P.; Xie, J. High efficiency microbial electrosynthesis of acetate from carbon dioxide using a novel graphene-nickel foam as cathode. *J. Chem. Technol. Biotechnol.* **2018**, *93*, 457–466. [[CrossRef](#)]
33. Zhang, Z.; Deng, X.; Sunarso, J.; Cai, R.; Chu, S.; Miao, J.; Zhou, W.; Shao, Z. Two-step fabrication of Li₄Ti₅O₁₂-coated carbon nanofibers as a flexible film electrode for high-power lithium-ion batteries. *ChemElectroChem* **2017**, *4*, 2286–2292. [[CrossRef](#)]

34. Wu, Y.; Yang, Y.; Zhao, X.; Tan, Y.; Liu, Y.; Wang, Z.; Ran, F. A novel hierarchical porous 3D structured vanadium nitride/carbon membranes for high-performance supercapacitor negative electrodes. *Nano-Micro Lett.* **2018**, *10*, 63. [[CrossRef](#)]
35. Li, Y.; Li, X.-M. Facile treatment of wastewater produced in Hummer's method to prepare Mn₃O₄ nanoparticles and study their electrochemical performance in an asymmetric supercapacitor. *RSC Adv.* **2013**, *3*, 2398–2403. [[CrossRef](#)]
36. Schönleber, M.; Uhlmann, C.; Braun, P.; Weber, A.; Ivers-Tiffée, E. A consistent derivation of the impedance of a lithium-ion battery electrode and its dependency on the state-of-charge. *Electrochim. Acta* **2017**, *243*, 250–259. [[CrossRef](#)]
37. Shrestha, N.; Chilkoor, G.; Wilder, J.; Ren, Z.J.; Gadhamshetty, V. Comparative performances of microbial capacitive deionization cell and microbial fuel cell fed with produced water from the Bakken shale. *Bioelectrochemistry* **2018**, *121*, 56–64. [[CrossRef](#)]
38. Somogyi, P.; Takagi, H. A note on the use of picric acid-paraformaldehyde-glutaraldehyde fixative for correlated light and electron microscopic immunocytochemistry. *Neuroscience* **1982**, *7*, 1779–1783. [[CrossRef](#)]
39. Zhao, Y.; Duan, L.; Hermanowicz, S.W. Influence of water transport characteristics on membrane internal conductive structure in forward osmosis microbial fuel cell. *J. Mol. Liq.* **2023**, *380*, 121704. [[CrossRef](#)]
40. Shrestha, N.; Chilkoor, G.; Xia, L.; Alvarado, C.; Kilduff, J.E.; Keating, J.J.; Belfort, G.; Gadhamshetty, V. Integrated membrane and microbial fuel cell technologies for enabling energy-efficient effluent Re-use in power plants. *Water Res.* **2017**, *117*, 37–48. [[CrossRef](#)] [[PubMed](#)]
41. Gao, Y.; Mohammadifar, M.; Choi, S. From microbial fuel cells to biobatteries: Moving toward on-demand micropower generation for small-scale single-use applications. *Adv. Mater. Technol.* **2019**, *4*, 1900079. [[CrossRef](#)]

Disclaimer/Publisher's Note: The statements, opinions and data contained in all publications are solely those of the individual author(s) and contributor(s) and not of MDPI and/or the editor(s). MDPI and/or the editor(s) disclaim responsibility for any injury to people or property resulting from any ideas, methods, instructions or products referred to in the content.